JGR Earth Surface

RESEARCH ARTICLE
10.1029/2024JF007691

Benford's Law as Debris Flow Detector in Seismic Signals

Qi Zhou[1,2], Hui Tang[1], Jens M. Turowski[1], Jean Braun[1,2], Michael Dietze[1,3], Fabian Walter[4], Ci-Jian Yang[5], and Sophie Lagarde[1,2]

[1]Helmholtz Centre Potsdam, GFZ German Research Centre for Geosciences, Potsdam, Germany, [2]Institute of Geosciences, University of Potsdam, Potsdam, Germany, [3]Faculty of Geoscience and Geography, Georg-August-Universität Göttingen, Göttingen, Germany, [4]Swiss Federal Institute for Forest, Snow and Landscape Research, Zürich, Switzerland, [5]Department of Geography, National Taiwan University, Taipei, Taiwan

Abstract Seismic instruments placed outside of spatially extensive hazard zones can be used to rapidly sense a range of mass movements. However, it remains challenging to automatically detect specific events of interest. Benford's law, which states that the first non-zero digit of given data sets follows a specific probability distribution, can provide a computationally cheap approach to identifying anomalies in large data sets and potentially be used for event detection. Here, we select vertical component seismograms to derive the first digit distribution. The seismic signals generated by debris flows follow Benford's law, while those generated by ambient noise do not. We propose the physical and mathematical explanations for the occurrence of Benford's law in debris flows. Our finding of limited seismic data from landslides, lahars, bedload transports, and glacial lake outburst floods indicates that these events may follow Benford's Law, whereas rockfalls do not. Focusing on debris flows in the Illgraben, Switzerland, our Benford's law-based detector is comparable to an existing random forest model that was trained on 70 features and six seismic stations. Achieving a similar result based on Benford's law requires only 12 features and single station data. We suggest that Benford's law is a computationally cheap, novel technique that offers an alternative for event recognition and potentially for real-time warnings.

Plain Language Summary Natural hazards, such as debris flows and landslides, pose a significant threat to the exposed communities. Seismic instruments are seen as effective tools for detecting these hazardous processes and may be used in early warning systems. However, the difficulty lies in identifying the events of interest concisely and objectively. Our study explores Benford's law, describing the relative occurrence of the first non-zero digit. We collected seismic data generated by various hazard events and compared the observed first-digit distribution with their agreement with Benford's law. We found seismic signals of debris flows follow Benford's law during the run-out phase, while ambient noise do not. Our detector, based on Benford's law and designed for debris flow, which is a computationally cheap and novel model, performs similarly to a machine learning algorithm previously used in the study site. Our work illustrates a new approach to detecting events and designing warning systems.

Key Points:

- The first-digit distribution of seismic signals generated by debris flows follows Benford's law
- When Benford's law appears, seismic signals tend to increase exponentially and converge to a power law distribution with exponent one
- A computationally cheap and novel detector based on Benford's law is developed for debris-flow events

Supporting Information:

Supporting Information may be found in the online version of this article.

Correspondence to:

Q. Zhou,
qi.zhou@gfz-potsdam.de

Citation:

Zhou, Q., Tang, H., Turowski, J. M., Braun, J., Dietze, M., Walter, F., et al. (2024). Benford's law as debris flow detector in seismic signals. *Journal of Geophysical Research: Earth Surface*, *129*, e2024JF007691. https://doi.org/10.1029/2024JF007691

Received 17 FEB 2024
Accepted 22 AUG 2024

Author Contributions:

Conceptualization: Qi Zhou, Hui Tang, Jens M. Turowski
Data curation: Michael Dietze, Fabian Walter, Sophie Lagarde
Methodology: Qi Zhou, Hui Tang, Jens M. Turowski
Supervision: Hui Tang, Jens M. Turowski, Jean Braun, Michael Dietze
Validation: Qi Zhou, Ci-Jian Yang
Writing – original draft: Qi Zhou
Writing – review & editing: Qi Zhou, Hui Tang, Jens M. Turowski, Jean Braun, Michael Dietze, Fabian Walter, Ci-Jian Yang, Sophie Lagarde

1. Introduction

Mass movements (e.g., landslide and debris flow) and extreme fluvial processes (e.g., flash floods and glacier lake outburst floods) are of significant concern in populated mountain areas, as they can cause huge loss of life and damage to civil infrastructure each year (Holub & Hübl, 2008; Merz et al., 2021; Regmi et al., 2015). Classification criteria for mass movements may vary depending on the focus of interest (Coussot & Meunier, 1996; Nemčok et al., 1972). Yet, the most widespread and destructive mass movements are generally considered to be debris flows, landslides, and rockslides (Dowling & Santi, 2014; Froude & Petley, 2018). Despite extensive efforts to mitigate their hazard through risk assessment and structural measures (Dai et al., 2002; Fuchs et al., 2007; Huebl & Fiebiger, 2005), the intricate geological conditions and dynamic processes of mass movements frequently pose challenges in preventing property damage and fatalities (Fan et al., 2019; Kean et al., 2019; Tiwari et al., 2022).

Early warning systems are an established approach to mitigating the impact of mass movements (Guzzetti et al., 2020; Hürlimann et al., 2019; Schlunegger et al., 2009). For example, systems based on measured rainfall intensity and predefined thresholds for triggering alarms (Baum & Godt, 2010; Marra et al., 2016) are among the most commonly employed warning approaches. However, maintaining rain gauges and obtaining accurate

rainfall intensity data in real time is challenging for the operation of a warning system, especially for catchments with large elevation differences. Inaccurate measurements and uncertainty in data interpolation lead to significant errors in rainfall thresholds (Nikolopoulos et al., 2015). In addition, due to the variability in geological and hydrological conditions, empirical thresholds for triggering debris flows and landslides are not transferable between catchments (Gregoretti et al., 2016; Wilson & Wieczorek, 1995). Detecting specific events of interest from time-series signals is essential for releasing a warning. Force plates, radar, laser, and video cameras are the most common sensors used for monitoring in early warning systems (Comiti et al., 2014; McArdell et al., 2007). However, some of these devices (e.g., force plates and radar sensors) require a high-power supply and regular maintenance, or can be easily destroyed by the hazard processes.

Continuous seismic and acoustic signals offer a new way to monitor mass movements with high temporal resolution (Cook & Dietze, 2022; Dietze, Mohadjer, et al., 2017; Dietze, Turowski, et al., 2017; Farin et al., 2019; Hübl et al., 2013; Le Breton et al., 2021; Li et al., 2024). The instruments can be installed outside the zones affected by the hazard and are thus in lesser danger of being destroyed. An array of seismic stations can help to detect and locate extreme, mass movement events on a regional scale (Cook et al., 2021; Ekström & Stark, 2013; Hammer et al., 2012). However, a seismic station records all ground vibration signals within its bandwidth, blending events of interest and those considered as noise. Current seismology-based detectors of mass movements and fluvial processes, such as seismic attribute-based methods (Dietze et al., 2022; Govi et al., 1993; Schimmel & Hübl, 2016; Wei & Liu, 2020), short-term average to long-term average ratio (Coviello et al., 2019), random forests (Hibert et al., 2017; Provost et al., 2017), and hidden Markov models (Dammeier et al., 2016; Hammer et al., 2012) require numerous waveform, spectral, network features or parameters to be fed into the model to identify events. In addition, collecting and labeling the data to parameterize or train such a model is time-consuming and requires experience. Applying these existing approaches to other sites requires re-training the model or calibrating the parameters. Worse, often no historical data are available for new sites to do this. Before warning systems can be constructed, implemented, and promoted, a convenient and portable approach to event detection must be found. Compared to ambient noise and signals not associated with extreme events in a natural environment, the temporal occurrence probability of mass movements is relatively low. Therefore, detecting debris flows and other mass movements in seismic time-series signals can be treated as anomaly detection.

The Newcomb–Benford law (BL) or the first-digit law, which is widely used in fraud and data quality detection, is a probability distribution of the first digit of a data set (Castañeda, 2011; Ley, 1996; Tam Cho & Gaines, 2007). Newcomb (1881) stated that the probability of occurrence of the first digits is such that the mantissae of their logarithms are equally probable:

$$P(d) = \log_{10}\left(1 + d^{-1}\right), \tag{1}$$

where $P(d)$ is the theoretical probability of the first none-zero digits, $d = [1, 2, \ldots, 9]$. For example, -0.01 and 100 share one as the same first digit with a likelihood of 0.301. Frank Benford rediscovered this relationship and tested it with 20 different data sets (Benford, 1938). It was later named after him as Benford's law. BL has been used in several fields of geosciences, such as in studying the homogeneity of natural hazard data sets and anomalies (Geyer & Martí, 2012; Joannes-Boyau et al., 2015). Earthquakes and Mars quakes were detected in seismic signals with BL (Díaz et al., 2015; Sambridge et al., 2010; Sun & Tkalčić, 2022). Due to the dimensionless nature and low computational cost of BL, it has the potential to be used to identify mass movements in seismic data at different catchments, perhaps even as a detector in data loggers.

In this study, we compiled seismic data generated by various mass movements and fluvial processes, calculated the first-digit distribution of seismic signals, and investigated which processes or periods follow BL. We propose some potential explanations for the BL appears in seismic signals generated by debris flows and not by ambient noise. Finally, we present a BL-based event detector for debris flows and compare its performance with a previously developed random forest model (Chmiel et al., 2021) for the same seismic network. Thus we show a novel approach for detecting mass movements and the potential for establishing a real-time warning system using BL.

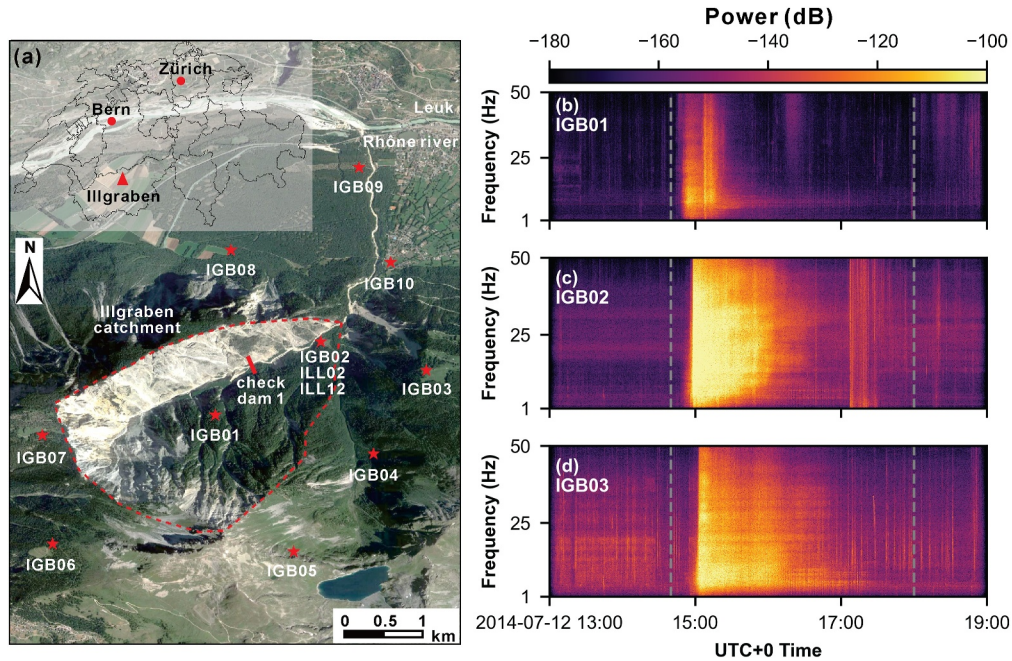

Figure 1. Study area and debris flow at Illgraben catchment, Switzerland. (a) The location and distribution of the temporary 9J seismic network (red stars and numbered as IGB) in the Illgraben catchment between 2012 and 2014. The detailed parameters of the three-component seismometers are described in Table S1 in Supporting Information S1. (b–d) Are the spectrograms of the vertical component (IGB01, IGB02, IGB03, respectively) for a debris flow event on 12 July 2014. UTC is the universal time coordinated. The gray dashed lines show the manually labeled event start (UTC+0 2014-07-12 14:40) and end (2014-07-12 18:00) times of this debris flow.

2. Data Source and Event Catalog

2.1. Study Site and Data Source

The Illgraben catchment near the village of Leuk, southwest Switzerland (Figure 1a) is one of the most active debris flow catchments in the Alps. It covers an area of about 9.5 km^2 and extends from the Rhône River at 610 m to the Illhorn Mountain, peaking at 2,716 m (Badoux et al., 2009). In the upstream trunk channel, the bare rock of limestones (north side of the main channel) and quartzites (south side) is susceptible to erosion and weathering and provides sediment for debris flows (Schlunegger et al., 2009). The Illgraben only accounts for less than 0.2% of the area of the Rhône valley but delivers more than 5% of sediment to the Rhône basin annually (Schlunegger et al., 2013). The annual rainfall is concentrated from May to October, and the Illgraben catchment roughly experiences three to five debris flows and several floods each year, mainly triggered by short-duration convective storms (McArdell et al., 2007). To mitigate the risk of debris flows and floods, a warning system has been implemented at the Illgraben that triggers an alarm when the number of impulses from an in-torrent ground vibration sensor exceeds empirically determined thresholds (Badoux et al., 2009). For additional details on the Illgraben, readers may refer to the works of Belli et al. (2022), Burtin et al. (2014), and Chmiel et al. (2021).

Considering that seismic data are not available for all stations for the whole year and the complexity of signals from stations far from the spatially propagating event, we mainly selected station IGB02 (same station location named as ILL02 in 2017 and ILL12 from 2018-now in the 9S seismic networks) for this study (Figure 1a), which is part of the 9J seismic networks deployed from 2012 to 2014 (Burtin et al., 2023; Zurich, 2012), closest to the channel and far from the nearby residential area of Leuk.

2.2. Event Catalog

To calculate the first-digit distribution of seismic signals and quantify which processes or periods follow BL, we examined 24 debris flows (one of which may be a flood event) that occurred in 2013–2014, and 34 debris flows (one of which may be a flood event) that occurred 2017–2020 in the Illgraben catchment (Table S2 in Supporting

Information S1). For the 2013–2014 debris flows, 10 of the 24 events were recorded by local warning systems (WSL events), and we manually labeled an additional 14 debris flows based on the event duration of waveforms and the 1–50 Hz features of the spectrogram (GFZ events, Text S1 in Supporting Information S1). One example of a debris flow that occurred on 12 July 2014, a WSL event, had high a signal-to-noise ratio SNR (Text S3 and Figure S14 in Supporting Information S1), and is shown in Figures 1b–1d. Unfortunately, no seismic data and event catalogs are available for the time between 2015 and 2016.

To complement the data with events from other locations and data for calculating the first-digit distribution, we added seismic signals from other mass movements and fluvial processes (Table S3 in Supporting Information S1), such as a 2013 rockfall event in the Illgraben, Switzerland (Burtin et al., 2016), a 2015 rockfall event in Lauterbrunnen, Switzerland (Dietze, Mohadjer, et al., 2017; Dietze, Turowski, et al., 2017), the 2014 Askja landslide, Iceland (Schöpa et al., 2018), a 2015 hurricane-induced lahar in Volcán de Colima, Mexico (Capra et al., 2018), a 2016 glacial lake outburst flood (GLOF) in Bhotekoshi, Nepal (Cook et al., 2018), a 2019 bedload transport event in the Taroko National Park (Turowski et al., 2022; Yang et al., 2024).

3. Methods

3.1. Data Preparation

To eliminate the long-period seismic signals and highlight events of interest, we demean, detrend, and apply a bandpass filter to the raw vertical-component (up-down) seismograms between 1 and 45 Hz (units are counts, processed by R package eseis 0.7.3 and Obspy 1.4.0). We then select a non-overlapping moving window to compute the probability distribution of digits one to nine and check whether the observed distribution adheres to BL (see Section 3.2). The number of data points (n) for each window is equal to the moving window length (W_L, units are seconds) multiplied by the seismic signal sampling frequency (f_s, units are Hertz, Tables S1 and S3 in Supporting Information S1 for details):

$$n = W_L \times f_s. \tag{2}$$

For each window, amplitude data points less than 100 counts will be discarded to improve the difference between background and event (refer to Section 5.4).

3.2. First-Digit Distribution and Benford's Law

We used two established statistical methods, the Kolmogorov-Smirnov test (Feller, 1948; Kaiser, 2019) and the Mann-Whitney U rank test (Mann & Whitney, 1947), to validate whether the observed first-digit distribution follows BL. The hypothesis is that the frequency of the observed first digits is not distinct from the theoretical BL values, or both represent the same distribution. We define that a p-value greater than 0.95 at least for any test means acceptance of the hypothesis. The observed first-digit distribution is considered to be consistent with BL if the hypotheses of two tests are accepted. In addition, the goodness of fit ϕ introduced by Sambridge et al. (2010) is used to evaluate the difference between the observed distribution and BL:

$$\phi = \left\{1 - \left(\sum_{d=1}^{9} \frac{\left(P(d)_{obs} - P(d)\right)^2}{P(d)}\right)^{1/2}\right\} \times 100\%, \tag{3}$$

where $P(d)_{obs}$ and $P(d)$ are the observed digit frequency and theoretical probability of BL, $d = [1, 2,\ldots, 9]$. A value of ϕ closer to one means that the distribution is closer to the theoretical BL value. To investigate the occurrence of BL in seismic signals, we examine the relationship between the time series of seismic signals and their corresponding first-digit distribution. This analysis allows us to understand the underlying factors contributing to the emergence of BL during specific processes or periods. For the processes or periods that follow BL, we examine the relationship between the time series of seismic signals and their first-digit distribution to investigate in what condition BL appears. In the time domain, the seismic waveform $S(t)$ is a function of time t and can be described with an interquartile range IQR as magnitude changes of the measurements. Here, one to 5 minutes of seismic signals before the maximum IQR were selected to fit an exponential curve for the increased parts (Text S2 in Supporting Information S1 for details):

$$S(t) = a \times e^{b \times t} + c, \tag{4}$$

$$IQR = Q_{75} - Q_{25}. \tag{5}$$

Previous studies have demonstrated that datasets-data index (sorted from smallest to largest) with a power law relationship (exponent one) satisfy BL, such as the data on many hydrological phenomena (Nigrini & Miller, 2007). We assume that the seismic data in all one-minute moving windows follow such a power law distribution. The data of each window were selected and sorted from smallest to largest (rank order) to calculate α by Equations 6 and 7 based on its magnitude (Newman, 2005). We will discuss the relationship between power law with exponent one and BL in Section 5.3.

$$p(x) = C \times x^{-\alpha}, \tag{6}$$

$$\alpha = 1 + n\left(\sum_{i=1}^{n} \ln \frac{x_i}{x_{\min}}\right)^{-1}. \tag{7}$$

Where $p(x)$ is the seismic data in any one-minute moving windows. C and α are the coefficients of the power law function. x_i, and $x_{\min}$ are the i-th data and minimum data in the data set of length n.

3.3. Data Preparation Debris Flow Detector Implementation

To demonstrate the application of BL, we developed a two-fold debris flow classification detector based on the supervised machine learning algorithm random forest (RF) (Breiman, 2001) and seismic data. RF is a decision tree-based model that has been successfully used for automated event classification from seismic signals (Chmiel et al., 2021; Hibert et al., 2017; Provost et al., 2017). Twelve input features were selected for this model, observed probability $P(d)_{obs}$ of first digit 1–9 in waveforms, interquartile range IQR, goodness of fit ϕ, and power law exponent α. Each feature was computed in a one-minute, non-overlapping moving window as used previously.

We divided the time series data set into a training data set (2017–2019, including 22 DF events) and a validation data set (2020, including 12 DF events). The temporal proportion of DF events (positive, labeled as one) and background noise (negative, labeled as zero) is roughly 0.004 (2130:509760, units are minutes), 0.008 (1452:181440, units are minutes) for training and validation, respectively. First, the time series training data set was fed into the RF model to train the detector (scikit-learn Version 1.3.0, Pedregosa et al. (2011)), then we used the time series validation data set to test the trained detector. As not all data windows from the DF periods follow BL, we also sliced the validation data set into 1212 segments, containing 12 DF events (positive, labeled as one) and 1200 background noise events (negative, labeled as zero). For segments of DF, the manually labeled start and end time stamps captured DF events from the time series seismic data, and for segments of background noise, the random temporal start time stamps captured noise events from the non-DF period with random durations ranging from 30 to 180 min.

We used a confusion matrix and $F1$ score to evaluate our detector performance. A true positive (TP) is an event that is classified as a debris flow by observation and our detector. A true negative (TN) is an event that is not classified as a debris flow by either observation or our detector. An event is labeled false positive (FP) when it is labeled as a debris flow by our detector but considered as a non-debris-flow event in observation. An event is labeled as false negative (FN) when an observed debris flow is not classified as debris flow by the detector. A good classification model should maximize the number of true-positive predictions and minimize the number of false-positive and false-negative predictions:

$$F1 = \frac{2\mathrm{TP}}{2\mathrm{TP} + \mathrm{FN} + \mathrm{FP}}. \tag{8}$$

To benchmark the performance of our detector, we opted to compare it to an existing random forest model (Chmiel et al., 2021). The referenced model was trained on seismic data from 2017 to 2019 and tested with 2020 data, and their model used data from six stations within the 9S seismic network and 70 seismic features.

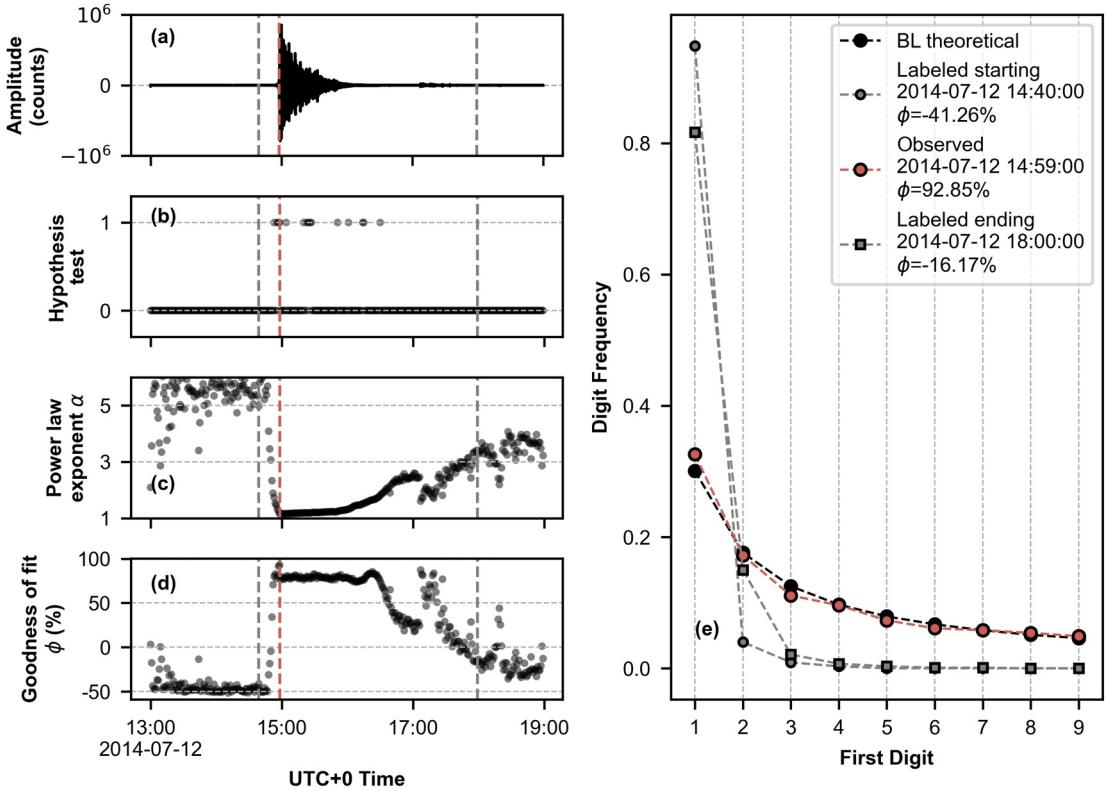

Figure 2. First-digit distribution of seismic signal generated by a debris flow in Illgraben on 2014-07-12 (data source: vertical-component of IGB02 station in 9J network). (a) Seismic waveforms were processed by demeaning, detrending, and band-pass filtering between 1 and 45 Hz. (b) Hypothesis test. One means that the *p*-value of both the Kolmogorov-Smirnov test and the Mann-Whitney U rank test is greater than 0.95 at least; otherwise, the value is zero. (c) Power law exponent. (d) Goodness of fit. (e) First-digit distribution of different time periods.

4. Results

4.1. Benford's Law and Seismic Signals

BL was observed in 57 (exclude 2020-06-10) out of the 58 labeled events in the Illgraben catchment between 2013–2014 and 2017–2020 (as shown in Figure S1 in Supporting Information S1). In addition, BL was observed during short time periods outside the five manually labeled debris flow events (Figure S1 in Supporting Information S1). These events occurred on 2014-05-23, 2014-05-24, and 2014-05-27 with GFZ label, as well as on 2014-07-08 and 2014-07-23 with WSL label. In the debris flow events that follow BL, we observed that both the Kolmogorov-Smirnov tests and the Mann-Whitney U rank test accept the hypothesis during the run-out phase. For example, the debris flow event on 12 July 2014 exhibits $\alpha_{\min}$ of 1.17, $\phi_{optimal}$ of 93.11% and suggests that the first-digit distribution of seismic signals follows BL (Figure 2). In addition, for other mass movements in our data set, the first-digit distribution of the seismic signal generated by the landslide (Figure S2 in Supporting Information S1) and the lahar (Figure S3 in Supporting Information S1) also exhibit BL. The two rockfall cases failed to follow BL (Figures S4–S6 in Supporting Information S1).

For fluvial processes in the Illgraben catchment, the flood case that occurred on 29 July 2013, followed BL (Figure S1 in Supporting Information S1), whereas the flood that occurred on 10 June 2020, did not exhibit BL distribution (Figure S1 in Supporting Information S1). In terms of fluvial processes, bedload transport complies with BL in the seismic signal (Figure S8 in Supporting Information S1), and the 2016 Bhotekoshi GLOF event can also be distinguished by BL (Figure 3). The 2016 Bhotekoshi GLOF can be conceptualized as a hazard chain that includes the breach of Gongbatongshacuo Lake, the landslide induced by the outburst along the river, and the failure of the hydropower intake dam (Cook et al., 2018), the BL does not currently allow for sufficient precision in differentiating these processes.

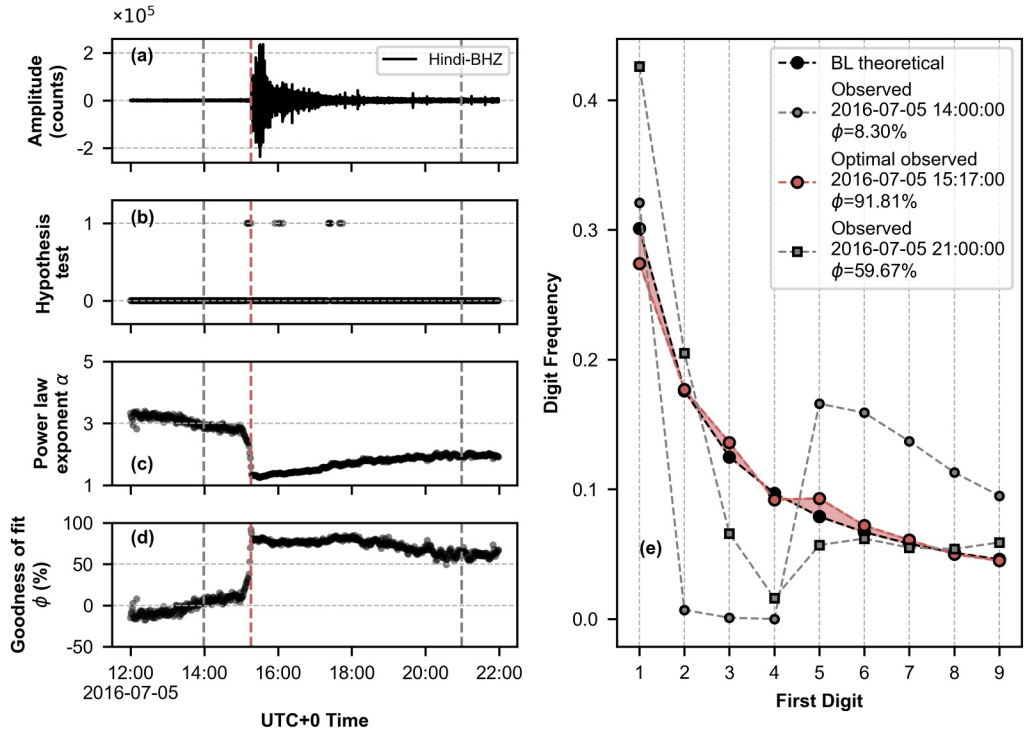

Figure 3. First-digit distribution of seismic signal generated by a glacial lake outburst flood GLOF in Bhotekoshi on 2016-07-05 (data source: vertical-component of Hindi station, Cook et al. (2018)). (a) Seismic waveforms were processed by demeaning, detrending, and band-pass filtering between 1 and 45 Hz. (b) Hypothesis test. One means that the *p*-value of both the Kolmogorov-Smirnov test and the Mann-Whitney U rank test is greater than 0.95 at least; otherwise, the value is zero. (c) Power law exponent. (d) Goodness of fit. (e) First-digit distribution of different time periods. The amplitude data point of waveform less than 500 counts was discarded.

4.2. Empirical Analysis for BL

As the debris flow front approaches, the *IQR* rapidly increases in the time series domain (Figure 4a), and we observed a good fit between seismic signals *S* and time *t* using the exponential function. The kernel density and coefficient of determination R^2 were used to show the exponential fitting difference between the event (IQR_{max} period) and noise (manually labeled event start time period). The averaged R^2 of 2013–2014 WSL (WSL1), 2017–2019 WSL (WSL2), and 2020 WSL (WSL3) label events are 0.904, 0.825, 0.772 respectively, and the averaged R^2 of 2013–2014 GFZ label events is 0.704 (Figures 4b and 4c, Table S2 in Supporting Information S1). However, the same fitting method did not yield an exponential curve for the noise period (Table S2 in Supporting Information S1 for details).

In addition, we observed that α for the 52 debris flow events (exclude 2014-05-23, 2014-05-24, 2014-05-27, 2014-07-08, 2014-07-23, and 2020-06-10) that follow BL only during the event phase ranged from 1.152 to 1.709 (Table S2 in Supporting Information S1 for details), which is much closer to one than during the noise period (Figures 4e and 4f). For instance, the event 2014-07-12 has $\alpha = 1.153$. Landslide, lahar, GLOF, and bedload transport case, which follow BL, share $\alpha = 1.112$–1.717 close to one during the moving process (Figure 4d). However, the exponent of two rockfall cases and most ambient noise is much higher than one for the whole period. Note that the processing of the seismic data affects α, which will be discussed later.

4.3. Debris-Flow Detector Based on BL

Without complex training and configuration of RF parameters, the results of training from 2017 to 2019 show that the input BL features are effective ($F1 = 0.9979$) in capturing debris flow events (Figure 5a). Given that not all DF periods follow BL, it is not surprising to observe that the trained detector, which receives a false negative rate of 0.5028 and a false positive rate of 0.1163 from the 2020 time series validation data set, cannot perfectly identify

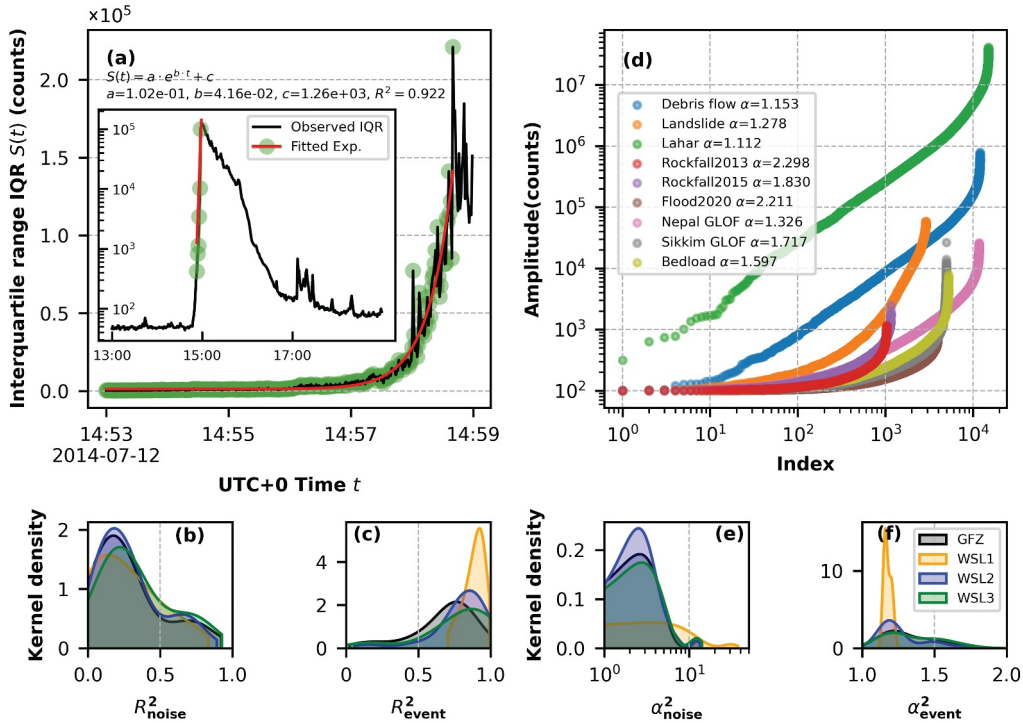

Figure 4. Correlation between seismic signals and BL. (a) Changes in the seismic signals for a debris flow event on 12 July 2014 and exponential fitting (Exp. fitting). (b, c) are the kernel density of the exponential fitting R^2. (d) Power law relationship in waveforms. (e, f) are the kernel density of the power law exponent α. The data displayed in panels (b, c, e, f) correspond to the maximum IQR period during 52 BL-followed debris flow events (Table S2 in Supporting Information S1 for details).

debris flows during the complete manually labeled period (Figures 5b and 8b, 8f). When the trained detector was fed the segments and applied a threshold to relabel the results from the model predicted class, there was a significant enhancement for the detectors, for example, $F1$ improved from 0.6395 to 1 (Figures 5c and 5d). For example, set threshold as 12 in Figure 5c, a segment is only classified as model predicted positive (debris flow) if the detector model outputs at least 12 times within this segment, otherwise, this segment is classified as model predicted negative (none DF).

5. Discussion

5.1. BL in Some Seismic Data Sets

The results show that BL is an efficient approach for detecting mass movements (e.g., landslide and debris flow) and some fluvial processes (e.g., GLOF and bedload transport) in vertical (up-down) component seismic data. Furthermore, it was observed that the horizontal (east-west E, north-south N) components seismic signals generated by debris flows also follow the BL and do not show a significant difference compared to the vertical component (Figures 6 and S13 in Supporting Information S1). However, due to the varying distances between the impact source and the seismic stations, the data collected within the same seismic network may not all follow BL (Figures S12–S13 in Supporting Information S1). The processes that follow BL (e.g., debris flow, landslide, lahar, GLOF, and bedload transport) usually contain more kinetic energy than cases that do not follow BL (e.g., ambient noise and rockfall cases). For rockfall that do not follow BL, we argue that the short event duration or low SNR make it difficult to distinguish between an event and ambient noise (Text S3, and Figures S5, S7, S14 in Supporting Information S1). Generally, the low SNR is due to geometric spreading and anelastic attenuation, the energy and amplitude of the signals dissipate during propagation, especially for high-frequency waves (Battaglia & Aki, 2003; Tsai & Atiganyanun, 2014). It is expected that data collected from a short source-receiver distance or a high sampling frequency sensor (e.g., ≥200 Hz) will assist in the examination of this hypothesis.

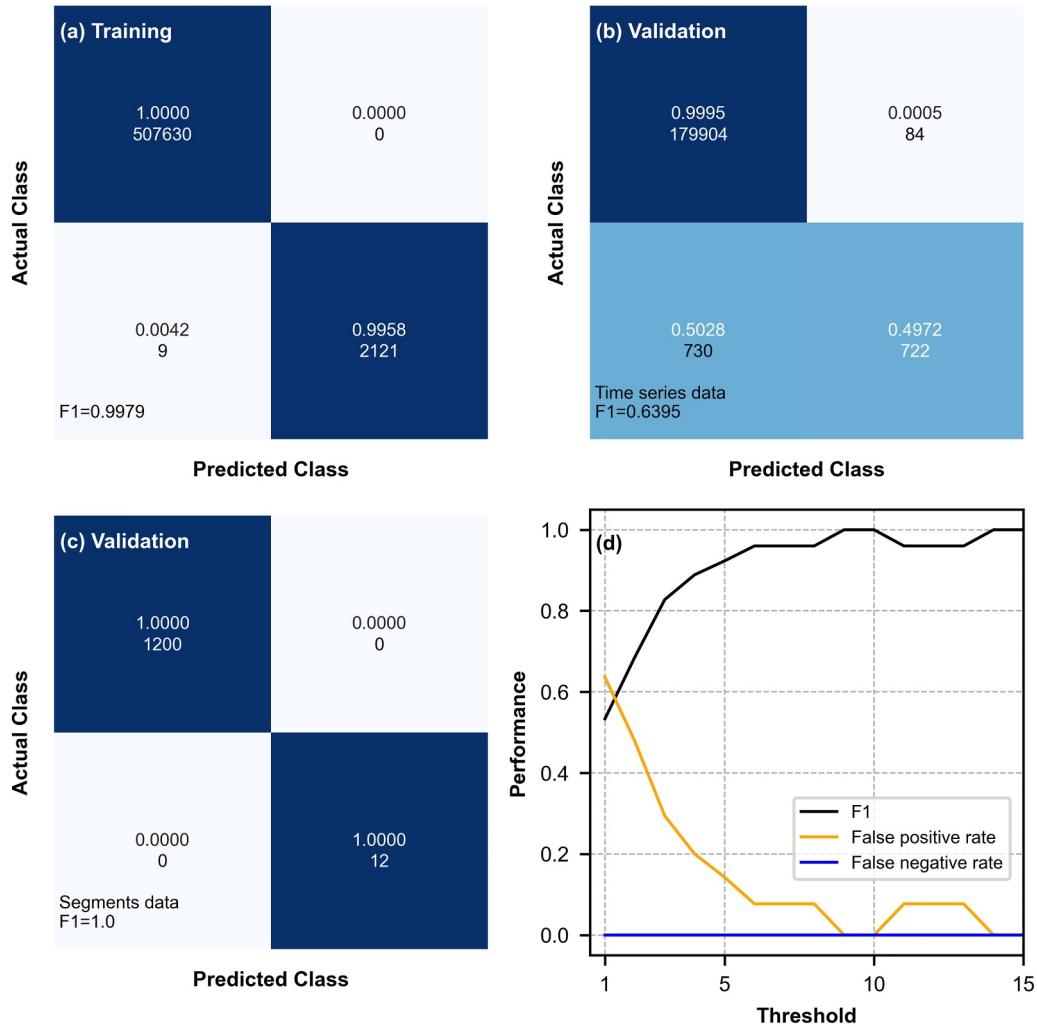

Figure 5. Normalized confusion matrix by actual class and detector performance. (a) Training results from 2017 to 2019 time series data sets. (b) Validation results from 2020 time series data sets. (c) Validation results from 2020 segments. (d) Detector performance under different thresholds. The false positive rate and False negative rate are FP/(FP + TN), and FN/(FN + TP), respectively.

Nevertheless, further seismic data are required to ascertain whether the landslides, lahars, GLOFs, rockfalls, and bedload transport follow BL or not.

5.2. Physical Explanation of Seismic Data Sets Following BL

For seismic data sets, Sambridge et al. (2010) first stated that a sufficient dynamic range of a regular signal may lead to a first-digit distribution following BL (e.g., seismic signals generated by an earthquake). However, that claim is not always correct (Berger & Hill, 2011). In theory, data sets crossing several orders of magnitude do not necessarily follow BL (Figure 7a); in practice, we found that the seismic signals that at least cross two orders of magnitude within a one-minute window follow BL (*IQR* 340 counts, Figure S7 in Supporting Information S1). For teleseismic events and local seismicity, using both natural and artificial data, Díaz et al. (2015) observed that compliance to BL does not depend primarily on the dynamic amplitude range, but rather relates to changes in frequency content. Yet, it is nearly impossible to obtain seismic signals in the field in which only frequency changes, without changes in the dynamic range. Seismic signals generated by mass movements or fluvial processes usually have significant changes in both magnitude (> two orders) and frequency (>1 Hz change in central frequency) when compared to an earthquake (Figures 1b, 1d, and 2a). In theory, the sole change in the frequency domain does not necessarily cause compliance to BL (Figure 7b).

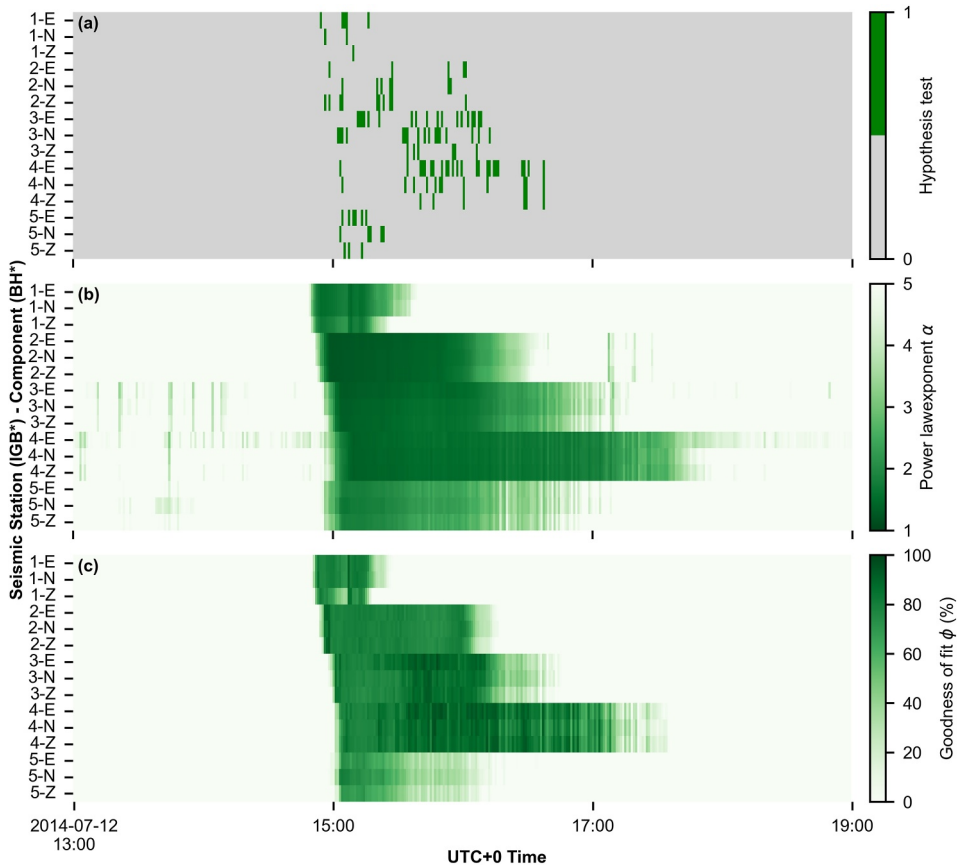

Figure 6. Testing Benford's law with data from different seismic stations (abbreviated as IGB*) and components (abbreviated as E, N, Z). (a) Hypothesis test. One means that the *p*-value of both the Kolmogorov-Smirnov test and the Mann-Whitney U rank test is greater than 0.95 at least; otherwise, the value is zero. (b) Power law exponent. (c) Goodness of fit. The amplitude data point of waveform less than 1,000 counts was discarded. The 1-E in label y denotes that the results are based on the east-west component of IGB01. The spectrogram is shown in Figure S11 in Supporting Information S1.

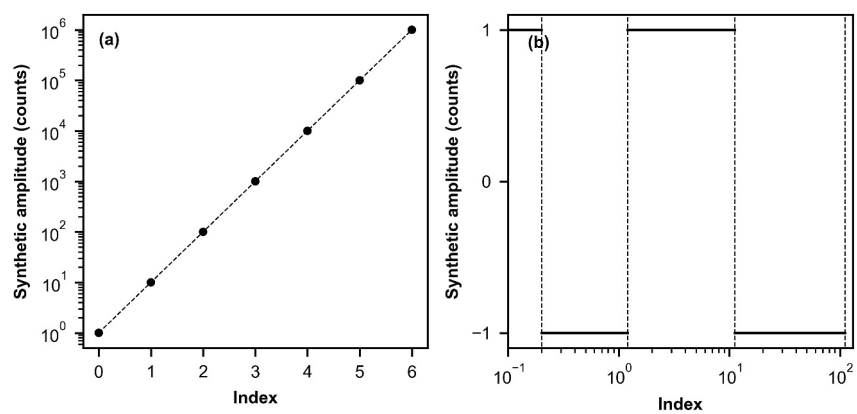

Figure 7. Synthetic amplitude data set. (a) Data sets [1, 10, …, 10^7] with a first digit of 1 that spans 7 orders of magnitude but do not follow BL. (b) A segment of synthetic amplitude with the first digit one and different frequencies. 0.1 Hz (index from 0.1 to 0.2), 1 Hz (index from 0.2 to 1.2), 10 Hz (index from 1.2 to 11.2), and 100 Hz (data index from 11.2 to 111.2).

5.3. Mathematical Explanation for Why Seismic Data Sets Follow BL

In addition to the physical explanations why seismic signals follow BL, we report here two mathematical explanations for the appearance of BL in seismic signals from statistics. When data adheres to BL, it also follows Zipf's law (Newman, 2005). BL appears exactly when the scaling exponent α in Zipf's law is equal to 1 (Pietronero et al., 2001). Consequently, so empirical values of the exponent close to one in seismic data will yield compliance to BL. In Equations 9–12 below, we provide a simple version of the proof for this statement. We assume a given data set X is a data set with data x follows Zipf's law or power law for continuous variables as:

$$p(x) \propto \frac{1}{x^{\alpha}} \quad \text{or} \quad p(x) = b \times x^{-\alpha}, \quad \text{where, } x \in X[x_1, x_2, \ldots, x_{n-1}, x_n] \tag{9}$$

where x is the frequency rank, $p(x)$ is its frequency, and b is a constant. Then, we can compute the first digit probability of the first digit by estimating the same relative probability for the various integers and dropping the constant b as:

$$P(N) = \int_{N}^{N+1} p(x)dx = \int_{N}^{N+1} x^{-\alpha}dx, \quad \text{where, } N = 1, 2, \ldots, 8, 9 \tag{10}$$

where $P(N)$ denotes the probability of digit N. When $\alpha = 1$, we have:

$$P(N) = \int_{N}^{N+1} x^{-1}dx = \int_{N}^{N+1} d(\log x) = \log\left(1 + \frac{1}{N}\right), \tag{11}$$

which is the precisely BL. When $\alpha \neq 1$, we obtain a generalized BL as:

$$P(N) = \int_{N}^{N+1} x^{-\alpha}dx = \frac{1}{1-\alpha}\left[(N+1)^{(1-\alpha)} - N^{(1-\alpha)}\right]. \tag{12}$$

Further, BL appears for a data set that rises or falls exponentially in time, which corresponds to a mapping from a linear to a logarithmic space (e.g., Figure 4a). Mathematically, BL can be derived from the exponential function as follows. Let's assume that a given data set X is an exponential evolving variable following the function $f(t) = \lambda e^{-\lambda t}$ for $t > 0$. The probability of the first digit $d = [1, 2, \ldots, 8, 9]$ in X could be calculated as $g_d(\lambda)$:

$$X = \bigcup_{k=-\infty}^{\infty} \left[d10^k, (d+1)10^k\right], \tag{13}$$

$$g_d(\lambda) = \sum_{k=-\infty}^{\infty} \int_{d10^k}^{(d+1)10^k} f(t)dt = \sum_{k=-\infty}^{\infty} e^{-\lambda d10^k}\left(1 - e^{-\lambda 10^k}\right) \tag{14}$$

Note that $g_d(\lambda) = g_d(10\lambda)$, and if we put the λ axis on the logarithmic scale, the $g_d(\lambda)$ will be a periodic function as $h_d(x) = g_d(10^x)$. Consequently, $h_d(x)$ can be written as a Fourier series as:

$$h_d(x) = \sum_{n} c_n e^{2\pi i n x}, \tag{15}$$

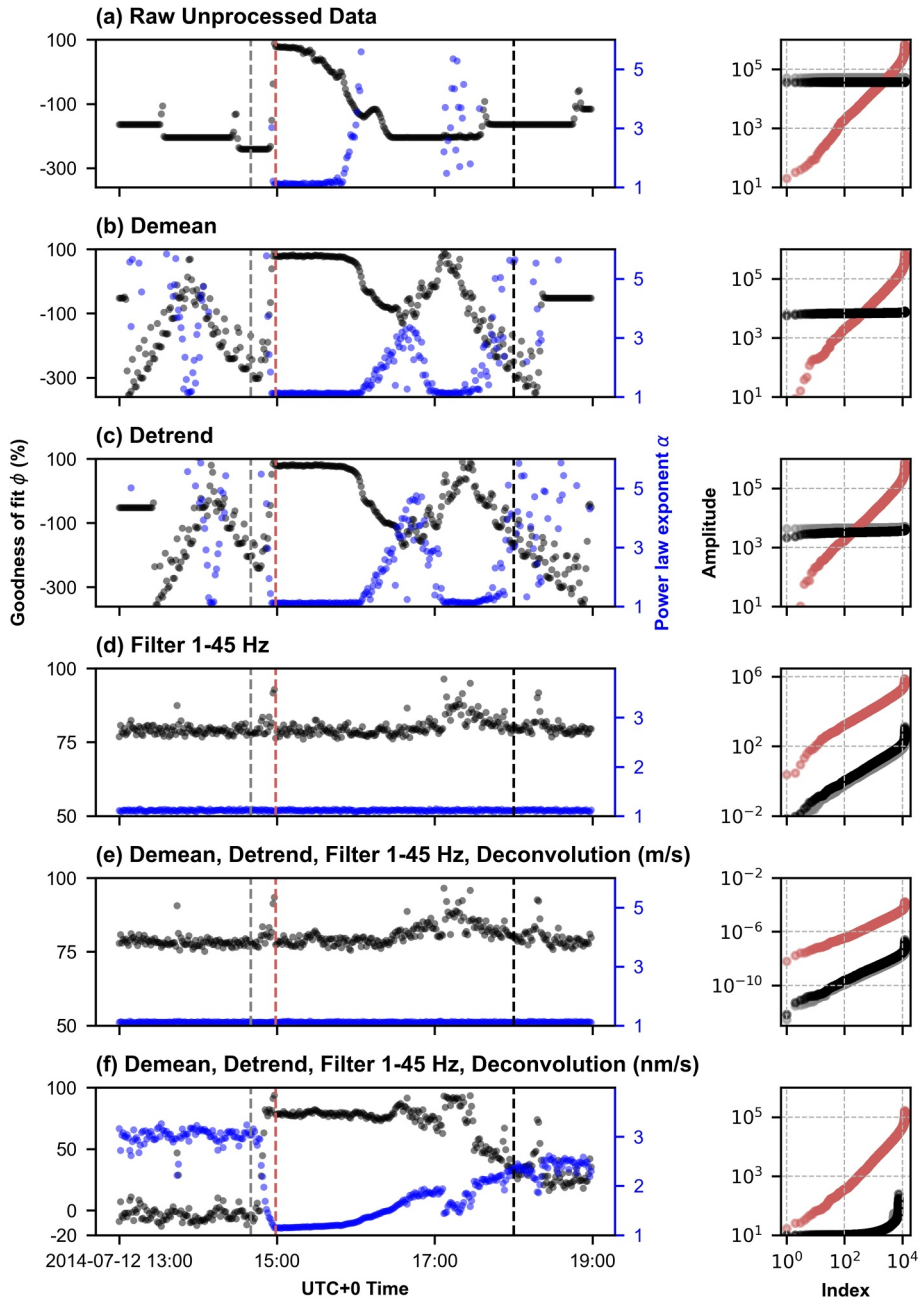

Figure 8. Seismic data processing methods and their effect on BL detection. (a–f) are the seismic signals processing methods using raw, detrended, demeaned, band-pass filtered 1–45 Hz, deconvoluted data sets (m/s), deconvoluted data sets (nm/s), respectively. The amplitude data for the vertical panel on the right is selected from the same three-time stamps in Figure 2, as shown by the dashed line in the vertical panel on the left. Amplitudes in panels (a–d) are in units of counts, in panel (e) are in units of m/s, and in panel (f) are in units of nm/s. Amplitudes less than 10 nm/s are discarded in panel (f).

$$c_n = \begin{cases} \log\left(1+\frac{1}{d}\right), & \text{if } n = 0 \\ \int_{-\infty}^{-\infty} e^{-d10^x}\left(1-e^{-d10^x}\right)e^{-2\pi i n x}, & \text{if } n \neq 0 \end{cases} \quad (16)$$

Finally, we obtain BL by calculating the integral mean of $h_d(x)$ similar to the previous derivations:

$$\begin{aligned} \text{mean}(h_d) &= \int_0^1 h_d(x)dx = c_0 \\ &= \log_{10}\left(1 + \frac{1}{N}\right). \end{aligned} \tag{17}$$

For strict proofs and mathematical derivations, see Engel and Leuenberger (2003) and Cong et al. (2019). We conclude that seismic signals that show an exponential increase in time can be expected to follow BL.

5.4. BL and Seismic Signals Generated by Surface Processes

We suggest that events with an exponentially rising signal that follow BL, do so primarily because of their spatial mobility. The amplitude of an approaching seismic source, dominated by surface waves, is controlled by the ground quality factor as an exponential term and the source-receiver distance as the inverse square root of the distance. As long as the distance at which a process emits sufficient energy to be detected by a seismometer is much larger than the channel-sensor distance (Figure 1a), a fast-moving mass that emits a constant seismic signal will produce data that sufficiently closely follows an exponential increase (Dietze et al., 2022), and is therefore in agreement with BL. In other words, BL is an efficient detector of fast approaching seismic sources at the landscape scale.

In practice, the methods of processing seismic signals may alter the difference between BL in ambient noise and the event phase and influence the performance of our detector. The demeaning and detrending do not change the seismic dynamic range or data distribution (Figures 8a–8c). But applying a band-pass filter or correcting for the instrument response will change the dynamic range and force the data set to follow a power law distribution (Figures 8d and 8e). That is why we discard data sets with less than 100 counts for debris flow to ensure that we differentiate between event and background noise using BL (Figures 2c and 2d). However, this number may need to be adjusted for different local background noise levels and sensor types. For example, the 2014-05-23, 2014-05-24, and 2014-05-27 events follow BL outside of the event period with less than 100 counts discarded (Figure S1 in Supporting Information S1), and the lahar requires an increase of the threshold to 10,000 (Figure S3 in Supporting Information S1). This suggests that using the raw data collected with the same instrument as ours or carefully determining the threshold at which the data will be discarded is necessary before applying BL to detect events from seismic signals. If a different instrument or configuration collected the data from the event of interest, it might be advisable to convert the amplitudes from meters per second (m/s) to nanometers per second (nm/s) and discard amplitudes less than 10 nm/s after removing the instrumental response.

5.5. Application of BL as an Early Warning Tool

BL is a computationally cheap and novel approach to detect debris flow for establishing early warning systems. Since only the first digit distribution needs to be calculated, the computation time for input feature or parameter calculation and model evolution is reduced. By simply placing a seismic station next to a debris flow channel, such as station IGB02 in the 9J network, we expect that BL can be applied in different sites without retraining the detector because of BL's non-dimensional input features and its general applicability. In practice, a BL-based early warning system can be implemented using data from two or three seismic stations along the main flow path to detect and cross-validate events. For instance, the debris flow event on 12 July 2014, was detected earlier by the IGB01 station upstream, with subsequent detection by downstream IGB02 and IGB03 stations exhibiting the same trend (Figures 2a–2d and 9). Training the detector with the ILL12 data from 2017 to 2019 and without any correction or retraining, it can successfully identify the event using the time series data from the 2014 IGB01 and IGB03 stations (Figure 9). Data from other catchments will be necessary to test how our detector responds to different geometry and seismic network characteristics. Nevertheless, our approach could be a simplified version of a debris flow event detector for triggering or turning on high-power supply and data transmission devices to catch events, such as radar and laser, for full-scale warning.

Our purpose in this paper is to explore the potential of BL as a prerequisite to develop an operational event detector or warning system for debris flows, which can also be adapted to other processes. An efficient real-time warning system requires the rapid detection of the event of interest, and signal processing plays a critical role in

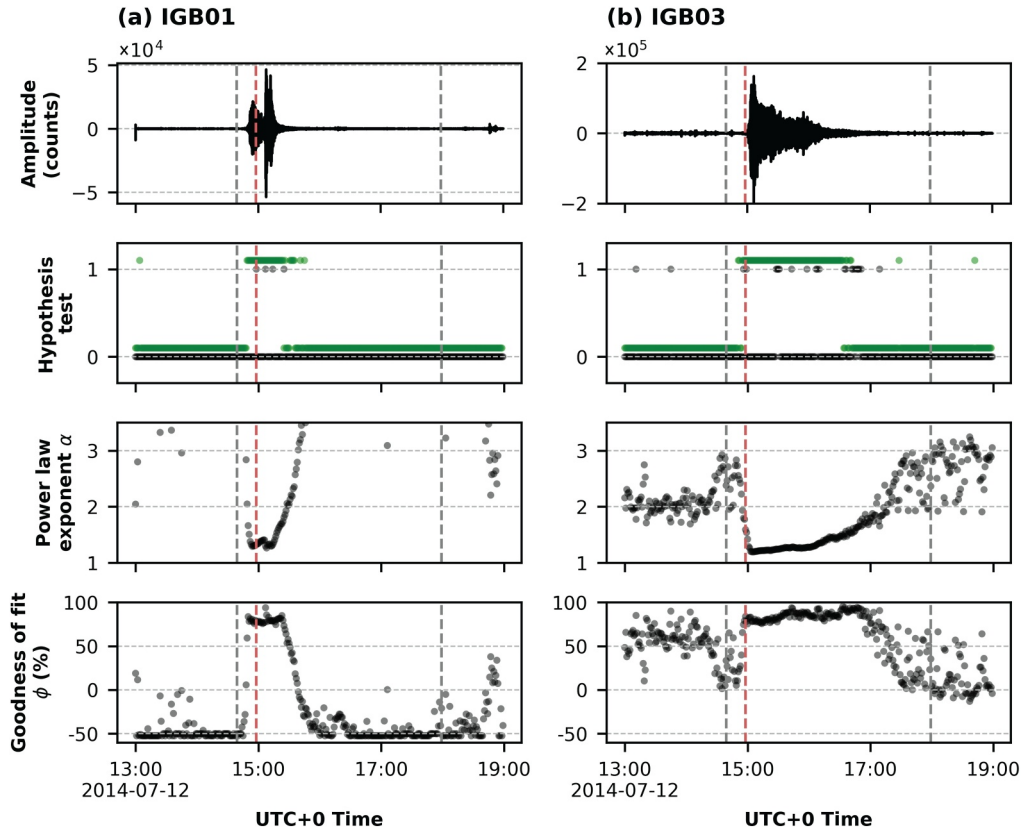

Figure 9. Detector model predicted results and BL features of the seismic signal generated by a debris flow in Illgraben on 2014-07-12 (data source: 9J network). (a, b) are results from IGB01 and IGB03 seismic stations. The dashed lines are the same time stamps in Figure 2. Green dots in the Hypothesis test panel denote the model-predicted debris flow time stamps.

validating seismology-driven warning systems (Arattano et al., 2014, 2016; Coviello et al., 2015). By using BL features for the random forest model, mass movement processes lasting longer than a few minutes can be reliably distinguished from background noise. Our model achieves a detection accuracy of 1.0 for both debris flow and non-debris flow events during the validation of segmental data based on 12 BL features and one seismic station. Our detection accuracy results are at least comparable to an existing random forest model calibrated in the same catchment by Chmiel et al. (2021), their model gives 0.83 and 0.94 for debris flows before or after check dam 1 (marked in Figure 1a) and 0.92 for non-debris-flow events, respectively. But their model was trained using 70 input features, including 25 waveform features, 17 spectral features, 17 spectrogram features, and 11 network features, and data collected from six seismic stations, and tested in near-real time with 2020 data. Our model is limited in distinguishing the entire debris flow period because not all time-phases follow BL. When utilizing machine learning algorithms for early warning of debris flow, it is not purely a classification task, since we are more interested in the event initiation periods rather than the entire process. Our detector model efficiently fulfills this goal, the debris flow initiation period can be well detected as displayed in Figure 9, but further study is required to explore this idea using a comprehensive seismic network. Data from more mass movements are needed to help understanding the scope of application of BL. Our study suggests that a single seismic station could efficiently detect events such as debris flow that moves continuously in the channel. However, the BL approach neglects frequency domain information, which could be used to improve the identification of the types of mass movements or fluvial processes.

6. Conclusion

Detecting events of interest from seismic signals to establish early warning systems is critical for hazard mitigation. In this study, we demonstrated that the first-digit distribution of seismic signals generated by debris flow follows Benford's law, and proposed the physical and mathematical explanations for the occurrence. Furthermore,

our results from limited seismic data indicate that landslides, lahars, bedload transports, and glacial lake outburst floods may follow Benford's law, while rockfalls do not. Our BL feature offers a less computationally intensive and novel approach for extracting anomalous energetic events, such as debris flows and landslides, from massive seismic signals. Moreover, the mass movement detector provides a promising strategy for building warning systems using seismic signals to mitigate hazards. In the future, we will collect more types of mass movement to calculate their first digit distribution to confirm whether they follow BL and develop a seismic network-based detector and implement our method for real-time detection.

Data Availability Statement

The seismic data collected from the 9J Network between 2013 and 2014 and the 9S Network between 2017 and 2020 are available for open access (Burtin et al., 2023; Zurich, 2012). The seismic data generated by rockfall (Burtin et al., 2023; Dietze, Mohadjer, et al., 2017), GLOF (Cook et al., 2018), and bedload transport (Turowski et al., 2022) events presented in this work are open access. The seismic data generated by landslide (Schöpa et al., 2018) and lahar (Capra et al., 2018) are upon request from Robert S. White (University of Cambridge), and Lucia Capra (Universidad Nacional Autónoma de México). The trained random forest model, the code utilized for the processing of seismic data and the calculation of Benford's law, is accessible from Zhou (2024) and GitHub (https://github.com/Nedasd/Benfords_law_as_mass_movements_detector.git).

Acknowledgments

The authors thank Ahmed Abdelwahab from the University of Potsdam who labeled the 2013–2014 debris flow data. We acknowledge Velio Coviello (Geo-Hydrological Protection CNR) and Lucia Capra (Universidad Nacional Autónoma de México) for providing the raw Mexico lahar seismic data, and Robert S. White (University of Cambridge) for providing the raw Askja landslide data. This study was funded by the State Key Laboratory of Geohazard Prevention and Geoenvironment Protection Open Fund (SKLGP2023K003), the National Natural Science Foundation of China (42120104002), and the first author is supported by the China Scholarship Council.

References

Arattano, M., Abancó, C., Coviello, V., & Hürlimann, M. (2014). Processing the ground vibration signal produced by debris flows: The methods of amplitude and impulses compared. *Computers & Geosciences*, *73*, 17–27. https://doi.org/10.1016/j.cageo.2014.08.005

Arattano, M., Coviello, V., Abancó, C., Hürlimann, M., & McArdell, B. W. (2016). Methods of data processing for debris flow seismic warning. *International Journal of Erosion Control Engineering*, *9*(3), 114–121. https://doi.org/10.13101/ijece.9.114

Badoux, A., Graf, C., Rhyner, J., Kuntner, R., & McArdell, B. W. (2009). A debris-flow alarm system for the alpine Illgraben catchment: Design and performance. *Natural Hazards*, *49*(3), 517–539. https://doi.org/10.1007/s11069-008-9303-x

Battaglia, J., & Aki, K. (2003). Location of seismic events and eruptive fissures on the piton de la fournaise volcano using seismic amplitudes. *Journal of Geophysical Research*, *108*(B8). https://doi.org/10.1029/2002jb002193

Baum, R. L., & Godt, J. W. (2010). Early warning of rainfall-induced shallow landslides and debris flows in the USA. *Landslides*, *7*(3), 259–272. https://doi.org/10.1007/s10346-009-0177-0

Belli, G., Walter, F., McArdell, B., Gheri, D., & Marchetti, E. (2022). Infrasonic and seismic analysis of debris-flow events at Illgraben (Switzerland): Relating signal features to flow parameters and to the seismo-acoustic source mechanism. *Journal of Geophysical Research: Earth Surface*, *127*(6), e2021JF006576. https://doi.org/10.1029/2021jf006576

Benford, F. (1938). The law of anomalous numbers. *Proceedings of the American Philosophical Society*, 551–572.

Berger, A., & Hill, T. P. (2011). Benford's law strikes back: No simple explanation in sight for mathematical gem. *The Mathematical Intelligencer*, *33*(1), 85–91. https://doi.org/10.1007/s00283-010-9182-3

Breiman, L. (2001). Random forests. *Machine Learning*, *45*(1), 5–32. https://doi.org/10.1023/a:1010933404324

Burtin, A., Hovius, N., McArdell, B., Turowski, J., & Vergne, J. (2014). Seismic constraints on dynamic links between geomorphic processes and routing of sediment in a steep mountain catchment. *Earth Surface Dynamics*, *2*(1), 21–33. https://doi.org/10.5194/esurf-2-21-2014

Burtin, A., Hovius, N., Turowski, J., Dietze, M., Lagarde, S., & McArdell, B. (2023). The 9J seismic network, 2012–2014 [Dataset]. *GFZ Data Services*. https://doi.org/10.14470/4W615776

Burtin, A., Hovius, N., & Turowski, J. M. (2016). Seismic monitoring of torrential and fluvial processes. *Earth Surface Dynamics*, *4*(2), 285–307. https://doi.org/10.5194/esurf-4-285-2016

Capra, L., Coviello, V., Borselli, L., Márquez-Ramírez, V.-H., & Arámbula-Mendoza, R. (2018). Hydrological control of large hurricane-induced lahars: Evidence from rainfall-runoff modeling, seismic and video monitoring [Dataset]. *Natural Hazards and Earth System Sciences*, *18*(3), 781–794. https://doi.org/10.5194/nhess-18-781-2018

Castañeda, G. (2011). La ley de benford y su aplicabilidad en el análisis forense de resultados electorales. *Politica y Gobierno*, *18*(2), 297–329.

Chmiel, M., Walter, F., Wenner, M., Zhang, Z., McArdell, B. W., & Hibert, C. (2021). Machine learning improves debris flow warning. *Geophysical Research Letters*, *48*(3), e2020GL090874. https://doi.org/10.1029/2020gl090874

Comiti, F., Marchi, L., Macconi, P., Arattano, M., Bertoldi, G., Borga, M., et al. (2014). A new monitoring station for debris flows in the European Alps: First observations in the Gadria basin. *Natural Hazards*, *73*(3), 1175–1198. https://doi.org/10.1007/s11069-014-1088-5

Cong, M., Li, C., & Ma, B.-Q. (2019). First digit law from Laplace transform. *Physics Letters A*, *383*(16), 1836–1844. https://doi.org/10.1016/j.physleta.2019.03.017

Cook, K. L., Andermann, C., Gimbert, F., Adhikari, B. R., & Hovius, N. (2018). Glacial lake outburst floods as drivers of fluvial erosion in the Himalaya [Dataset]. *Science*, *362*(6410), 53–57. https://doi.org/10.1126/science.aat4981

Cook, K. L., & Dietze, M. (2022). Seismic advances in process geomorphology. *Annual Review of Earth and Planetary Sciences*, *50*(1), 183–204. https://doi.org/10.1146/annurev-earth-032320-085133

Cook, K. L., Rekapalli, R., Dietze, M., Pilz, M., Cesca, S., Rao, N. P., et al. (2021). Detection and potential early warning of catastrophic flow events with regional seismic networks. *Science*, *374*(6563), 87–92. https://doi.org/10.1126/science.abj1227

Coussot, P., & Meunier, M. (1996). Recognition, classification and mechanical description of debris flows. *Earth-Science Reviews*, *40*(3–4), 209–227. https://doi.org/10.1016/0012-8252(95)00065-8

Coviello, V., Arattano, M., Comiti, F., Macconi, P., & Marchi, L. (2019). Seismic characterization of debris flows: Insights into energy radiation and implications for warning. *Journal of Geophysical Research: Earth Surface*, *124*(6), 1440–1463. https://doi.org/10.1029/2018jf004683

Coviello, V., Arattano, M., & Turconi, L. (2015). Detecting torrential processes from a distance with a seismic monitoring network. *Natural Hazards*, *78*(3), 2055–2080. https://doi.org/10.1007/s11069-015-1819-2

Dai, F., Lee, C. F., & Ngai, Y. Y. (2002). Landslide risk assessment and management: An overview. *Engineering Geology*, *64*(1), 65–87. https://doi.org/10.1016/s0013-7952(01)00093-x

Dammeier, F., Moore, J. R., Hammer, C., Haslinger, F., & Loew, S. (2016). Automatic detection of alpine rockslides in continuous seismic data using hidden Markov models. *Journal of Geophysical Research: Earth Surface*, *121*(2), 351–371. https://doi.org/10.1002/2015jf003647

Díaz, J., Gallart, J., & Ruiz, M. (2015). On the ability of the Benford's law to detect earthquakes and discriminate seismic signals. *Seismological Research Letters*, *86*(1), 192–201. https://doi.org/10.1785/0220140131

Dietze, M., Hoffmann, T., Bell, R., Schrott, L., & Hovius, N. (2022). A seismic approach to flood detection and characterization in upland catchments. *Geophysical Research Letters*, *49*(20), e2022GL100170. https://doi.org/10.1029/2022gl100170

Dietze, M., Mohadjer, S., Turowski, J. M., Ehlers, T. A., & Hovius, N. (2017). Seismic monitoring of small alpine rockfalls–validity, precision and limitations [Dataset]. *Earth Surface Dynamics*, *5*(4), 653–668. https://doi.org/10.5194/esurf-5-653-2017-supplement

Dietze, M., Turowski, J. M., Cook, K. L., & Hovius, N. (2017). Spatiotemporal patterns, triggers and anatomies of seismically detected rockfalls. *Earth Surface Dynamics*, *5*(4), 757–779. https://doi.org/10.5194/esurf-5-757-2017

Dowling, C. A., & Santi, P. M. (2014). Debris flows and their toll on human life: A global analysis of debris-flow fatalities from 1950 to 2011. *Natural Hazards*, *71*(1), 203–227. https://doi.org/10.1007/s11069-013-0907-4

Ekström, G., & Stark, C. P. (2013). Simple scaling of catastrophic landslide dynamics. *Science*, *339*(6126), 1416–1419. https://doi.org/10.1126/science.1232887

Engel, H.-A., & Leuenberger, C. (2003). Benford's law for exponential random variables. *Statistics & Probability Letters*, *63*(4), 361–365. https://doi.org/10.1016/S0167-7152(03)00101-9

Fan, X., Scaringi, G., Korup, O., West, A. J., van Westen, C. J., Tanyas, H., et al. (2019). Earthquake-induced chains of geologic hazards: Patterns, mechanisms, and impacts. *Reviews of Geophysics*, *57*(2), 421–503. https://doi.org/10.1029/2018rg000626

Farin, M., Tsai, V. C., Lamb, M. P., & Allstadt, K. E. (2019). A physical model of the high-frequency seismic signal generated by debris flows. *Earth Surface Processes and Landforms*, *44*(13), 2529–2543. https://doi.org/10.1002/esp.4677

Feller, W. (1948). On the Kolmogorov-Smirnov limit theorems for empirical distributions. *The Annals of Mathematical Statistics*, *19*(2), 177–189. https://doi.org/10.1214/aoms/1177730243

Froude, M. J., & Petley, D. N. (2018). Global fatal landslide occurrence from 2004 to 2016. *Natural Hazards and Earth System Sciences*, *18*(8), 2161–2181. https://doi.org/10.5194/nhess-18-2161-2018

Fuchs, S., Heiss, K., & Hübl, J. (2007). Towards an empirical vulnerability function for use in debris flow risk assessment. *Natural Hazards and Earth System Sciences*, *7*(5), 495–506. https://doi.org/10.5194/nhess-7-495-2007

Geyer, A., & Martí, J. (2012). Applying Benford's law to volcanology. *Geology*, *40*(4), 327–330. https://doi.org/10.1130/g32787.1

Govi, M., Maraga, F., & Moia, F. (1993). Seismic detectors for continuous bed load monitoring in a gravel stream. *Hydrological Sciences Journal*, *38*(2), 123–132. https://doi.org/10.1080/02626669309492650

Gregoretti, C., Degetto, M., Bernard, M., Crucil, G., Pimazzoni, A., De Vido, G., et al. (2016). Runoff of small rocky headwater catchments: Field observations and hydrological modeling. *Water Resources Research*, *52*(10), 8138–8158. https://doi.org/10.1002/2016wr018675

Guzzetti, F., Gariano, S. L., Peruccacci, S., Brunetti, M. T., Marchesini, I., Rossi, M., & Melillo, M. (2020). Geographical landslide early warning systems. *Earth-Science Reviews*, *200*, 102973. https://doi.org/10.1016/j.earscirev.2019.102973

Hammer, C., Beyreuther, M., & Ohrnberger, M. (2012). A seismic-event spotting system for volcano fast-response systems. *Bulletin of the Seismological Society of America*, *102*(3), 948–960. https://doi.org/10.1785/0120110167

Hibert, C., Provost, F., Malet, J.-P., Maggi, A., Stumpf, A., & Ferrazzini, V. (2017). Automatic identification of rockfalls and volcano-tectonic earthquakes at the piton de la fournaise volcano using a random forest algorithm. *Journal of Volcanology and Geothermal Research*, *340*, 130–142. https://doi.org/10.1016/j.jvolgeores.2017.04.015

Holub, M., & Hübl, J. (2008). Local protection against mountain hazards? State of the art and future needs. *Natural Hazards and Earth System Sciences*, *8*(1), 81–99. https://doi.org/10.5194/nhess-8-81-2008

Hübl, J., Schimmel, A., Kogelnig, A., Suriñach, E., Vilajosana, I., & McArdell, B. (2013). A review on acoustic monitoring of debris flow. *International Journal of Safety and Security Engineering*, *3*(2), 105–115. https://doi.org/10.2495/safe-v3-n2-105-115

Huebl, J., & Fiebiger, G. (2005). Debris-flow mitigation measures. In *Debris-flow hazards and related phenomena* (pp. 445–487). Springer Berlin Heidelberg. https://doi.org/10.1007/3-540-27129-5_18

Hürlimann, M., Coviello, V., Bel, C., Guo, X., Berti, M., Graf, C., et al. (2019). Debris-flow monitoring and warning: Review and examples. *Earth-Science Reviews*, *199*, 102981. https://doi.org/10.1016/j.earscirev.2019.102981

Joannes-Boyau, R., Bodin, T., Scheffers, A., Sambridge, M., & May, S. M. (2015). Using Benford's law to investigate natural hazard dataset homogeneity. *Scientific Reports*, *5*(1), 12046. https://doi.org/10.1038/srep12046

Kaiser, M. (2019). Benford's law as an indicator of survey reliability—Can we trust our data? *Journal of Economic Surveys*, *33*(5), 1602–1618. https://doi.org/10.1111/joes.12338

Kean, J. W., Staley, D. M., Lancaster, J. T., Rengers, F. K., Swanson, B. J., Coe, J. A., et al. (2019). Inundation, flow dynamics, and damage in the 9 January 2018 Montecito debris-flow event, California, USA: Opportunities and challenges for post-wildfire risk assessment. *Geosphere*, *15*(4), 1140–1163. https://doi.org/10.1130/ges02048.1

Le Breton, M., Bontemps, N., Guillemot, A., Baillet, L., & Larose, É. (2021). Landslide monitoring using seismic ambient noise correlation: Challenges and applications. *Earth-Science Reviews*, *216*, 103518. https://doi.org/10.1016/j.earscirev.2021.103518

Ley, E. (1996). On the peculiar distribution of the US stock indexes' digits. *The American Statistician*, *50*(4), 311–313. https://doi.org/10.2307/2684926

Li, Y., Cui, Y., Hu, X., Lu, Z., Guo, J., Wang, Y., et al. (2024). Glacier retreat in eastern Himalaya drives catastrophic glacier hazard chain. *Geophysical Research Letters*, *51*(8), e2024GL108202. https://doi.org/10.1029/2024gl108202

Mann, H. B., & Whitney, D. R. (1947). On a test of whether one of two random variables is stochastically larger than the other. *The Annals of Mathematical Statistics*, *18*(1), 50–60. https://doi.org/10.1214/aoms/1177730491

Marra, F., Nikolopoulos, E., Creutin, J., & Borga, M. (2016). Space–time organization of debris flows-triggering rainfall and its effect on the identification of the rainfall threshold relationship. *Journal of Hydrology*, *541*, 246–255. https://doi.org/10.1016/j.jhydrol.2015.10.010

McArdell, B. W., Bartelt, P., & Kowalski, J. (2007). Field observations of basal forces and fluid pore pressure in a debris flow. *Geophysical Research Letters*, *34*(7). https://doi.org/10.1029/2006gl029183

Merz, B., Blöschl, G., Vorogushyn, S., Dottori, F., Aerts, J. C., Bates, P., et al. (2021). Causes, impacts and patterns of disastrous river floods. *Nature Reviews Earth & Environment*, *2*(9), 592–609. https://doi.org/10.1038/s43017-021-00195-3

Nemčok, A., Pašek, J., & Rybář, J. (1972). Classification of landslides and other mass movements. *Rock Mechanics*, *4*(2), 71–78. https://doi.org/10.1007/bf01239137

Newcomb, S. (1881). Note on the frequency of use of the different digits in natural numbers. *American Journal of Mathematics*, *4*(1), 39–40. https://doi.org/10.2307/2369148

Newman, M. E. (2005). Power laws, Pareto distributions and Zipf's law. *Contemporary Physics*, *46*(5), 323–351. https://doi.org/10.1080/00107510500052444

Nigrini, M. J., & Miller, S. J. (2007). Benford's law applied to hydrology data—Results and relevance to other geophysical data. *Mathematical Geology*, *39*(5), 469–490. https://doi.org/10.1007/s11004-007-9109-5

Nikolopoulos, E., Borga, M., Creutin, J., & Marra, F. (2015). Estimation of debris flow triggering rainfall: Influence of rain gauge density and interpolation methods. *Geomorphology*, *243*, 40–50. https://doi.org/10.1016/j.geomorph.2015.04.028

Pedregosa, F., Varoquaux, G., Gramfort, A., Michel, V., Thirion, B., Grisel, O., et al. (2011). Scikit-learn: Machine learning in python. *Journal of Machine Learning Research*, *12*, 2825–2830.

Pietronero, L., Tosatti, E., Tosatti, V., & Vespignani, A. (2001). Explaining the uneven distribution of numbers in nature: The laws of Benford and Zipf. *Physica A: Statistical Mechanics and its Applications*, *293*(1–2), 297–304. https://doi.org/10.1016/s0378-4371(00)00633-6

Provost, F., Hibert, C., & Malet, J.-P. (2017). Automatic classification of endogenous landslide seismicity using the random forest supervised classifier. *Geophysical Research Letters*, *44*(1), 113–120. https://doi.org/10.1002/2016gl070709

Regmi, N. R., Giardino, J. R., McDonald, E. V., & Vitek, J. D. (2015). A review of mass movement processes and risk in the critical zone of earth. *Developments in Earth Surface Processes*, *19*, 319–362. https://doi.org/10.1016/b978-0-444-63369-9.00011-2

Sambridge, M., Tkalčić, H., & Jackson, A. (2010). Benford's law in the natural sciences. *Geophysical Research Letters*, *37*(22). https://doi.org/10.1029/2010gl044830

Schimmel, A., & Hübl, J. (2016). Automatic detection of debris flows and debris floods based on a combination of infrasound and seismic signals. *Landslides*, *13*(5), 1181–1196. https://doi.org/10.1007/s10346-015-0640-z

Schlunegger, F., Badoux, A., McArdell, B. W., Gwerder, C., Schnydrig, D., Rieke-Zapp, D., & Molnar, P. (2009). Limits of sediment transfer in an alpine debris-flow catchment, Illgraben, Switzerland. *Quaternary Science Reviews*, *28*(11–12), 1097–1105. https://doi.org/10.1016/j.quascirev.2008.10.025

Schlunegger, F., Norton, K., Caduff, R., & Shroder, J. (2013). Hillslope processes in temperate environments. *Treatise in Geomorphology*, *3*, 337–354.

Schöpa, A., Chao, W.-A., Lipovsky, B. P., Hovius, N., White, R. S., Green, R. G., & Turowski, J. M. (2018). Dynamics of the Askja Caldera July 2014 landslide, Iceland, from seismic signal analysis: Precursor, motion and aftermath [Dataset]. *Earth Surface Dynamics*, *6*(2), 467–485. https://doi.org/10.5194/esurf-6-467-2018

Sun, W., & Tkalčić, H. (2022). Repetitive marsquakes in Martian upper mantle. *Nature Communications*, *13*(1), 1695. https://doi.org/10.1038/s41467-022-29329-x

Tam Cho, W. K., & Gaines, B. J. (2007). Breaking the (Benford) law: Statistical fraud detection in campaign finance. *The American Statistician*, *61*(3), 218–223. https://doi.org/10.1198/000313007x223496

Tiwari, A., Sain, K., Kumar, A., Tiwari, J., Paul, A., Kumar, N., et al. (2022). Potential seismic precursors and surficial dynamics of a deadly Himalayan disaster: An early warning approach. *Scientific Reports*, *12*(1), 3733. https://doi.org/10.1038/s41598-022-07491-y

Tsai, V. C., & Atiganyanun, S. (2014). Green's functions for surface waves in a generic velocity structure. *Bulletin of the Seismological Society of America*, *104*(5), 2573–2578. https://doi.org/10.1785/0120140121

Turowski, J. M., Chen, W.-S., Queißer, T., Chang, J.-M., Chao, W.-A., Nativ, R., et al. (2022). Taiwan multi-parametric environmental seismic network [Dataset]. *GFZ Data Services*. https://doi.org/10.14470/GD993669

Wei, S.-C., & Liu, K.-F. (2020). Automatic debris flow detection using geophones. *Landslides*, *17*(2), 349–359. https://doi.org/10.1007/s10346-019-01258-9

Wilson, R. C., & Wieczorek, G. F. (1995). Rainfall thresholds for the initiation of debris flows at la Honda, California. *Environmental and Engineering Geoscience*, *1*(1), 11–27. https://doi.org/10.2113/gseegeosci.i.1.11

Yang, C.-J., Turowski, J. M., Zhou, Q., Nativ, R., Tang, H., Chang, J.-M., & Chen, W.-S. (2024). Measuring bedload motion time at second resolution using Benford's law on acoustic data. *Earth and Space Science*, *11*(7), e2023EA003416. https://doi.org/10.1029/2023ea003416

Zhou, Q. (2024). Supporting material for "Benford's law as debris flow detector in seismic signals" [Dataset]. *Zenodo*. https://doi.org/10.5281/zenodo.13373477

Zurich, S. S. S. S. A. E. (2012). 9s - Temporary deployments in Switzerland associated with landslides [Dataset]. *ETH Zurich*. https://doi.org/10.12686/SED/NETWORKS/XP